YMTHE, Volume *30*

Supplemental Information

PD-1 and TIGIT downregulation distinctly affect the effector and early memory phenotypes of CD19-targeting CAR T cells

Young-Ho Lee, Hyeong Ji Lee, Hyung Cheol Kim, Yujean Lee, Su Kyung Nam, Cedric Hupperetz, Jennifer S.Y. Ma, Xinxin Wang, Oded Singer, Won Seog Kim, Seok Jin Kim, Youngil Koh, Inkyung Jung, and Chan Hyuk Kim

Supplemental Materials and Methods

siRNA transfection

Stimulated T cells were transfected with 150 pmol siRNA at 1600 V for 10 ms with three pulses using the NEON transfection system (ThermoFisher). 24 hours later, knock-down efficiency was determined by flow cytometry. siRNA sequences, which can be converted shRNA, were listed in Supplementary Table 1. In the case of PD-1 and TIM-3, however, the shRNA screening process proceeded immediately, skipping the selection of optimal siRNA candidates.

CD266 knockout by Cas9 RNP

CD226 gRNA candidates, listed in Supplementary Table 2**,** were predicted using the CHOPCHOP and Cas-Designer tools. The gRNA sequence, which contains the T7 promoter sequence, ~20 nucleotides of CD226-specific sequence and a gRNA backbone sequence, was overlapped with the sgRNA scaffold oligonucleotide by overlapping PCR. For *in vitro* transcription (IVT), 1.4 μg PCR products were mixed with 50U T7 RNA polymerase (NEB), 1 U RNase inhibitor (NEB), 10 mM fresh DTT, 14 mM $MgCl_2$, and 4 mM of each ribonucleotide triphosphate (Jena Bioscience) and incubated at 37 °C overnight. For the eradication of DNA, 2 U DNase I (NEB) was added to IVT mixture and further incubated at 37 °C for 30 min. sgRNA was purified with the RNeasy MinElute Cleanup kit (Qiagen, 74204). sgRNA targeting the CAG (CMV-IE, chicken actin, rabbit beta globin) promoter was used as negative control. Cas9 RNPs were prepared immediately before electroporation by incubating 7 μg Cas9 (enzynomics, M058UL), and 14 μg synthetic sgRNA in 20 μM Hepes (pH 7.5), 150 mM KCl, 1 mM MgCl2, 10% (vol/vol) glycerol, and 1 mM TCEP at 37 °C for 10 min. Stimulated T cells were electroporated with the Neon™ transfection device and Transfection System 10 μl Kit (ThermoFisher, USA). $1.3x10^6$ cells were washed with PBS before resuspension in 8 μl T buffer. RNP and T cells were mixed and transferred to 10 μl Neon™ Tip, and electroporated with a Neon electroporation device (1,600V, 10ms, 3 pulses). The electroporated T cells were suspended with fresh complete T cell medium, and further incubated with a 5% CO_2 atmosphere at 37°C overnight. 24 hours post-electroporation, CD266 expression was

evaluated by flow cytometry. Editing efficiency was estimated by T7 endonuclease I (NEB) assay according to the manufacturer's instructions using the following primers: forward 5`-AAGTATCTTCCAGTTGGGTGTCCCA-3`, reverse 5`-GATTGATGGATTCACAAGATAAAGAAACCCTC-3`

Generation of patient-derived, clinical-grade CAR T cells

The collection of human T cells from the leukapheresis product of a DLBCL patient (F, 54 years old) with recurrent brain metastasis who was administered 5 cycle of rituximab, MTX, Vincristine, and procavaine, was approved by the Institutional Review Board of the Samsung Medical Center (IRB #2018-11-066). A pool of $CD4^+$ and $CD8^+$ T cells was isolated using CliniMACS CD4 and CD8 GMP MicroBeads (Miltenyi Biotec, Germany). GMP-grade lentiviruses, generated with 19BBz-nt, 19PBBz-nt, or 19PTBBz-nt constructs, were manufactured by Takara Bio and used to generate CAR T cells per manufacturing protocols developed by Curocell Inc.

Supplemental Table 1. shRNA and siRNA sequences

siRNA & shRNA	Sequences (5` → 3`)
GFP	TCTCGGCATGGACGAGCTGTA
PD-1 #1	CCTGTGGTTCTATTATATTAT
PD-1 #2	GCCTAGAGAAGTTTCAGGGAA
PD-1 #3	CATTGTCTTTCCTAGCGGAAT
TIM3 #3	GGAATTCGCTCAGAAGAAA
TIM3 #4	GGACCAAACTGAAGCTATATT
TIM3 #586	GGATCCAAATCCCAGGCATAA
TIM3 #1518	GGTGCTGAGGTGAAAGCATAA
TIM3 #2128	GCTTGTTGTGTGCTTGAAAGA
TIM3 #2015	GCACTGAACTTAAACAGGCAT
LAG3 #503	GATCTCAGCCTTCTGCGAAGA
LAG3 #1221	GGTCTTTCCTCACTGCCAAGT
LAG3 #1379	GCCACTGTCACATTGGCAATC
LAG3 #1465	TCCAGTATCTGGACAAGAACG
LAG3 #1702	GCTGTTTCTCATCCTTGGTGT
LAG3 #1751	GCCTTTGGCTTTCACCTTTGG
LAG3 #138	CCAGCTTTCCAGCTTTCCTCT
LAG3 #1092	GCTTCAACGTCTCCATCATGT
LAG3 #1278	CTGGAGACAATGGCGACTTTA
LAG3 #1616	GCAGCAGTGTACTTCACAGAG
LAG3 #1954	TCAGCAGCCCAGTCCAAATAA
TIGIT #268	GCTTCTGGCCATTTGTAATGC

TIGIT #2	GGGAGTACTTCTGCATCTATC
TIGIT #739	GCTGCATGACTACTTCAATGT
TIGIT #1	TAACGTGGATCTTGATCATAA
TIGIT #1386	GGAGACATACACAGGCCTTCA
TIGIT #1750	GCATTTGGGCCTTGATCTACC
CTLA4 #3	GGTGGAGCTCATGTACCCACC
CTLA4 #1	CCCAAATTACGTGTACTACAA
CTLA4 #1058	GCATCACTTGGGATTAATATG
CTLA4 #1154	GCGAGGGAGAAGACTATATTG
CTLA4 #1309	GCCAGTGATGCTAAAGGTTGT
CTLA4 #1686	GGTGGTATCTGAGTTGACTTG

Supplemental Table 2. CD226-targeting gRNA sequences

gRNA	Sequences (5` → 3`)
gRNA #1	AAAGTAGGATAATCCATCTC
gRNA #2	AGAGACATGTTCTCGGCAAA
gRNA #3	CTCTCTTTACACTTACCCAC
gRNA #4	GTTAAGAGGTCGATCTGACG

Supplemental Figure legends

Figure S1. Generation of PD-1-downregulated CAR T cells. (A) Transduction efficiency of CAR T cells transduced with empty (mock), GFP, or PD-1 shRNA #1-3-containing lentiviruses was determined as the percentage of ΔLNGFR$^-$positive cells. **(B)** Surface CAR expression was analyzed with APC-conjugated anti-mouse Fab antibody on day 6 after the LNGFR$^+$ isolation of transduced cells. Error bars represent the range from n = 2 independent donors in separate experiments.

Figure S2. Target cell expression of CD19, PD-L1, and CD80. Surface CD19, PD-L1, and CD80 expression levels of Nalm-6-GL-PD-L1-CD80, Nalm-6-GL-PD-L1, Nalm-6, K562-CD19-PD-L1, K562-CD19, and K562 cells was determined by flow cytometry.

Figure S3. PD-1 downregulation enhances the *in vivo* antitumor activity of CAR T cells in a manner dependent on target cell expression of PD-L1. 1x10^6 Nalm-6-GL or Nalm-6-GL-PD-L1 leukemia cells were injected intravenously into NSG mice. 5 days later, 1x10^6 CAR T cells were injected intravenously. Tumor burden was monitored based on the bioluminescence intensity from the IVIS imaging system. Data are from n = 2 mock-, n = 4 19GBBz-, and n = 4 19PBBz-treated Nalm-6-GL bearing mice and n = 3 mock-, n = 4 19GBBz-, and n = 4 19PBBz-treated Nalm-6-GL-PD-L1 bearing mice. Statistical analysis was done by unpaired two-tailed t-test on the results from day 40.

Figure S4. CD19 specific CAR expression level of 19G28z, 19GBBz, 19P28z, and 19PBBz cells. CAR and ΔLNGFR expression level of 19G28z, 19GBBz, 19P28z, and 19PBBz cells on day 6 following LNGFR$^+$ isolation. Bars represent the ranges from CAR T cells generated from two donors.

Figure S5. Kinetics of PD-1, CTLA-4, LAG-3, TIGIT, and TIM-3 expression in activated CD4 or CD8 T cells. PBMCs were stimulated with anti-CD3/CD28 beads. PD-1, LAG-3, TIGIT, and TIM-3 expression levels of CD4$^+$ and CD8$^+$ T cells were determined by flow cytometry on days 0, 3, 6, and 12 after stimulation. The CTLA-4 expression level was evaluated through intracellular staining.

Figure S6. Selection of 21-mer siRNA candidates targeting TIGIT, LAG-3, and CTLA-4. **(A)** Schematic representation of siRNA screening and selection. 150 pmol siRNA candidates were electroporated (Neon electroporation system, 1600V, 10ms, 3 pulses) into T cells 2 days after stimulation. The expression level of inhibitory receptors was evaluated by flow cytometry on day 4. siRNA targeting GFP was used as a negative control. **(B)** Representative FACS plots of TIGIT, LAG-3, and CTLA-4 expression in T cells electroporated with each siRNA.

Figure S7. Selection of shRNA candidates targeting TIM-3. (A) Schematic representation of the generation and analysis of *shTIM-3*-CD19 CAR constructs as described in Supplementary Figure 1. CD19-specific CAR T cells were stimulated with γ-irradiated K562-CD19 cells for 2 days and analyzed for the expression of TIM-3 by flow cytometry. **(B)** Representative FACS plots of TIM-3 expression in ΔLNGFR$^+$ CAR T cells expressing each TIM-3 targeting shRNA. shRNA targeting GFP (*shGFP*) was used as a negative control.

Figure S8. Knockdown efficiency of ICRs and CAR expression in CD19 specific CAR T cells. (A) Schematic representation of the generation of CD19-specific CAR T cells with selected shRNA sequences targeting TIM-3, TIGIT, LAG-3, and CTLA-4. ΔLNGFR$^+$ T cells were stimulated with γ-irradiated K562-CD19 cells on day 10 and knockdown efficiency was measured on day 12. **(B)** The expression level of inhibitory receptors in CAR T cells expressing the indicated shRNA cassetttes was evaluated by flow cytometry on day 12. **(C)** CAR expression levels in CAR T cells expressing the indicated shRNA cassettes were determined on day 10 by flow cytometry. Data are the pooled mean ± SD from two indepdendent experiments performed in duplicates . Statistical analysis was done by One-Way ANOVA. * $p < 0.05$, ** $p < 0.01$, *** $p < 0.001$, **** $p < 0.0001$.

Figure S9. Generation of CAR T cells with dual downregulation of inhibitory receptors. (A) The transduction efficiency of dual shRNA constructs was determined by measuring CD19 CAR ΔLNGFR expression by FACS on day 4 after transduction. **(B)** The gMFI of CD19-CAR in ΔLNGFR$^+$ T cells on day 10 after transduction. Data are from the mean ± SD from three donors. **(C)** CD112 or CD155 expression level in Raji, Nalm-6-GL-

PD-L1, K562-CD19-PD-L1, and IM-9 cells with or without IFN-γ treatment for 24 h. CD112 or CD115 expression **(D)** HLA-DR expression level in Nalm-6-GL-PD-L1 cells with or without IFN-γ treatment at the indicated doses for 24 hours. (**E)** The intracellular expression level of galectin-9 in Nalm-6-GL-PD-L1 cells. Statistical analysis was done by One-Way ANOVA. ns, not significant.

Figure S10. Analysis of tumor burden performed in Fig 3. (A) NSG mice were injected intravenously with 1×10^6 Nalm-6-GL-PD-L1 leukemia cells. 5 days later, 1×10^6 CAR T cells with dual downregulation (*shGFP*, *shPD-1_shGFP*, *shPD-1_shTIM-3*, *shPD-1_shTIGIT*, *shPD-1_shLAG-3*, *shPD-1_shCTLA-4*) were injected intravenously. Tumor burden was monitored using the bioluminescence IVIS imaging system for 89 days following tumor engraftment. **(B)** Nalm-6-GL-PD-L1 bearing mice were treated with 0.5×10^6 or 0.25×10^6 CAR T cells with PD-1 or PD-1/TIGIT downregulation. Tumor burden was monitored based on the bioluminescence intensity from the IVIS imaging system for 54 days following tumor engraftment.

Figure S11. Generation and characterization of 19GBBz, 19PBBz, 19TBBz, and 19PTBBz cells. (A) Schematic illustration of the vector constructs used to generate 19GBBz, 19PBBz, 19TBBz, and 19PTBBz CAR T cells. **(B)** Surface expression level of CD19 CAR was evaluated by flow cytometry on day 6 after isolation of transduced cells. Data are the pooled mean ± SD from two independent experiments performed in duplicates. **(C)** PD-1 and **(D)** TIGIT expression levels of 19GBBz, 19PBBz, 19TBBz, and 19PTBBz cells stimulated with γ-irradiated K562-CD19 cells for 2 days. Data are the pooled mean ± SD from two indepdendent experiments performed in duplicates. Statistical analysis was done by One-Way ANOVA. * $p < 0.05$, ** $p < 0.01$, *** $p < 0.001$, ns = not significant.

Figure S12. *CD226* knockout and its effect on the production of IL-2 in 19PTBBz cells. (A) Schematic representation of CD226 knockout by CRISPR/Cas9 and the flow cytometric evaluation of the expression level of CD226 following knockout by 4 different sgRNA candidates. sgRNA targeting CAG (CMV-IE, chicken actin, rabbit beta globin) was used as a negative control. **(B)** The knockout efficiency of gRNA #4 targeting CD226 was estimated by

T7 endonuclease I assay. **(C)** Schematic representation of the generation of CD226 KO CD19 specific CAR T cells and the measurement of intracellular IL-2 by flow cytometry. **(D)** Intracellular IL-2 expression levels in $CD226^+$ and $CD226^-$ populations measured by flow cytometry. Data are the mean ± SD from one experiment performed in triplicates.

Figure S13. CD112 and CD155 expression on CAR T cells. Expression levels of CD112 and CD155 in 19GBBz cells with or without CD3/CD28 stimulation for 2 days measured by flow cytometry.

Figure S14. Differentiation state of 19GBBz cells upon repeated stimulation *in vitro*. **(A)** 19GBBz cells were stimulated with γ-irradiated Nalm-6-GL-PD-L1-CD80 cells every six days. The differentiation state of $CD4^+$ and $CD8^+$ 19GBBz CAR T cells was determined by flow cytometry for CCR7 and CD45RO expression on day 10 after each stimulation. **(B)** Representative flow cytometry plot for CCR7 and CD45RO expression. Data are the mean ± range from two donors. T_{CM} = $CD45RO^+CCR7^+$ cells, T_{EM} = $CD45RO^+CCR7^-$ cells.

Figure S15. CD45RO and CCR7 expression in 19GBBz, 19PBBz, 19TBBz, and 19PTBBz cells. Representative flow cytometry plot of CD45RO and CCR7 expression in 19GBBz, 19PBBz, 19TBBz, and 19PTBBz cells on day 16 (10 days after 2nd stimulation) as shown in Fig. 4C.

Figure S16. Changes in the transcriptomic profile of 1st and 2nd stimulated CAR T cells. (A) Schematic representation of the timeline for 1st and 2nd stimulation and sample preparation for RNA-seq. **(B)** Pearson's correlation analysis of the transcriptomic profiles and **(C)** hierarchical clustering of differentially-expressed genes from 1st- and 2nd-stimulated 19GBBz cells derived from two donors (FDR $q \leq 0.05$). **(D)** Heat map of selected genes associated with T cell function in 1st- and 2nd- stimulated 19GBBz cells. Asterisks represent the statistical significance as measured by *q*-value. **€** Normalized Enrichment Scores (NESs) of significantly enriched gene sets associated with phenotypic and functional T cell signatures in 1st- and 2nd-stimulated 19GBBz cells as determined by GSEA analysis. * = $q < 0.05$, ** = $q < 0.01$, *** = $q < 0.001$, **** = $q < 0.0001$.

Figure S17. Generation and functional evaluation of healthy donor-derived, clinical-grade CD19-targeting CAR T cells. (A) Schematic representation of CAR T cell manufacturing in a semi-automated closed system. **(B)** Schematic representation of the vectors used to manufacture healthy donor-derived, clinical-grade CAR T cells. **(C)** NOG mice were injected intravenously with 1×10^6 Nalm-6-GL-PD-L1 cells. 5 days later, CAR^+ T cells (% CAR^+: 19BBz-nt 40.19 %; 19PBBz-nt 38.46 %; 19PTBBz-nt 42.10 %) were intravenously injected at the indicated doses. Tumor burden was monitored based on the bioluminescence intensity from the IVIS imaging system. Kaplan-Meier survival analysis with Log-rank (Mantel-Cox) test comparing each CAR T-treated group. Data are from n = 3 mock mice and n = 6 mice for all CAR T cell-treated groups.

Figure S18. Generation and characterization of patient-derived, clinical-grade CD19-targeting CAR T cells with dual PD-1/TIGIT downregulation. (A) Transduction efficiency of CAR^+ T cells on day 6 after transduction. **(B)** CD4/CD8 ratio of 19BBz-nt or 19PTBBz-nt cells on day 6 after transduction. **(C)** Expression of CD45RA and CCR7 to distinguish the differentiation state of 19BBz-nt or 19PTBBz-nt cells. **(D)** The absolute number of CAR T cells on day 6 after transduction. **€** Change in glucose concentration during the rapid expansion with the G-rex gas permeable culture device. **(F)** Knockdown efficiency of PD-1 and TIGIT. All data are the mean ± SD from three independent experiments. Statistical analysis was done by unpaired two-tailed t-test. T_N = $CD45RA^+CCR7^+$, T_{CM} = $CD45RA^-CCR7^+$, T_{EM} = $CD45RA^-CCR7^-$, T_{EFF} = $CD45RA^+CCR7^-$. nt = not tagged

Figure S19. The measurement of tumor weight. the tumor weight on day 28 of the $4x10^6$ CART injection group was measured, as shown in the luminescence data of figure 6H.

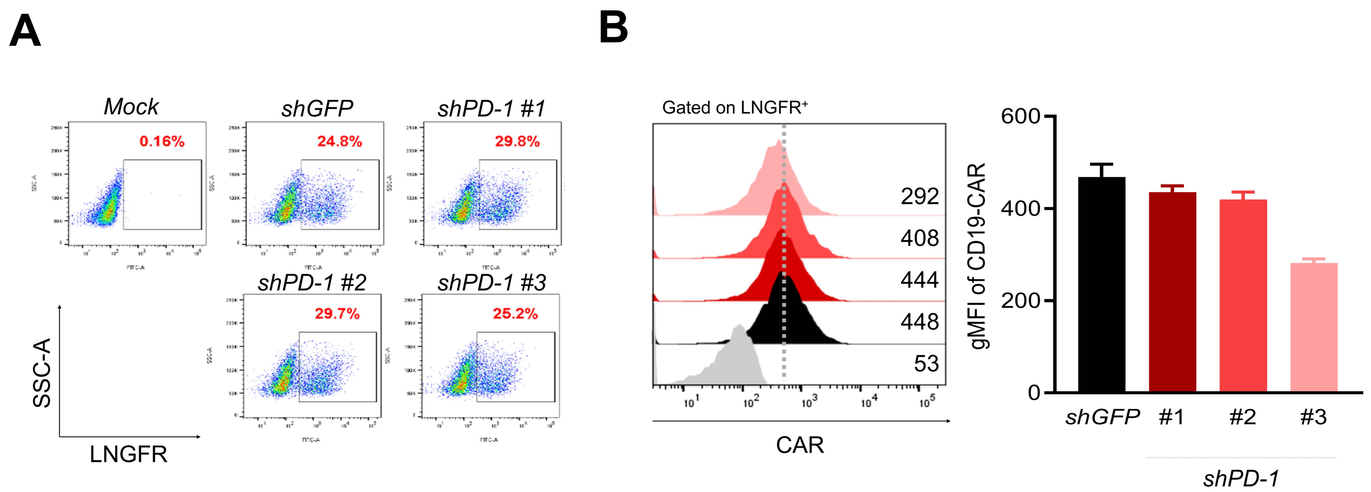

Supplementary figure 1

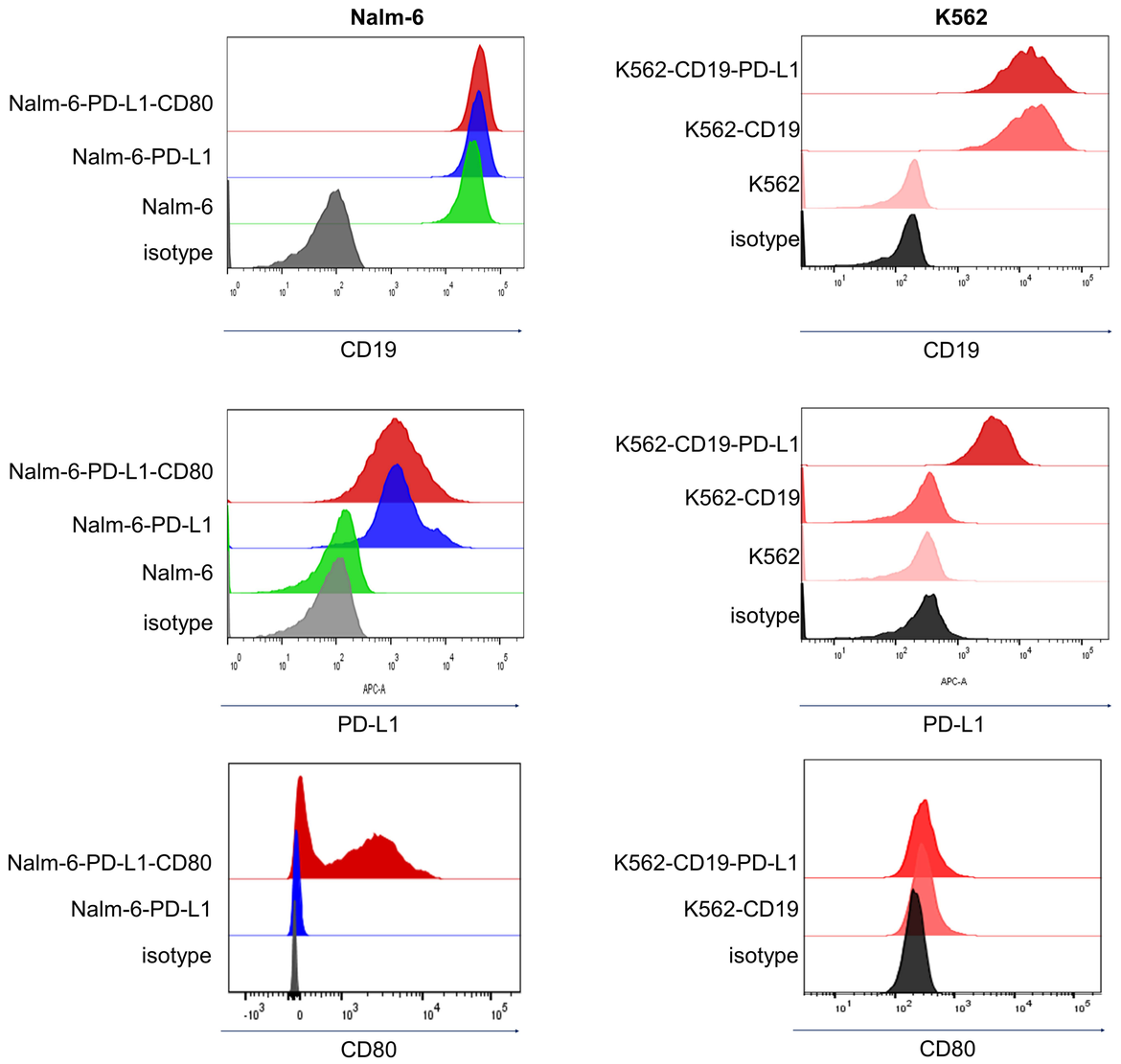

Supplementary figure 2

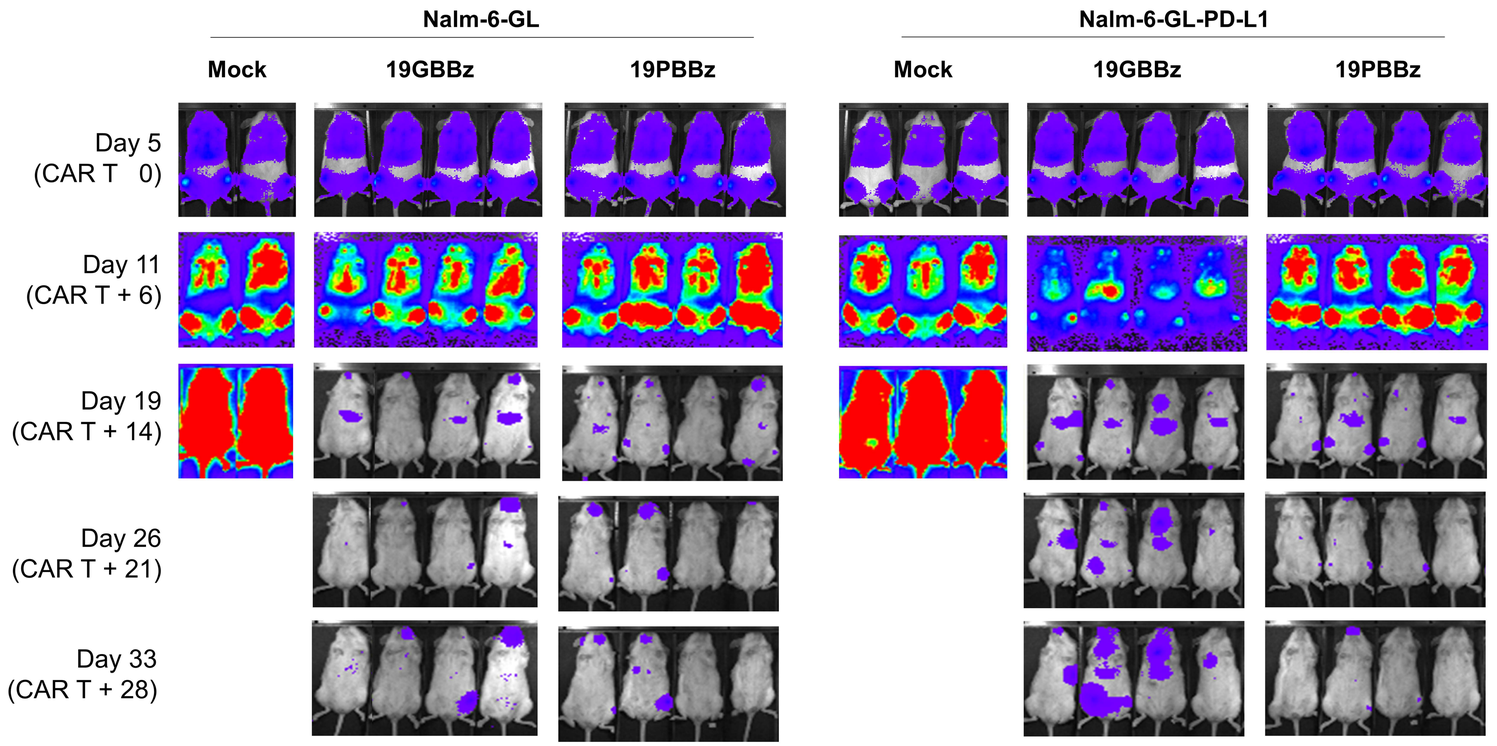

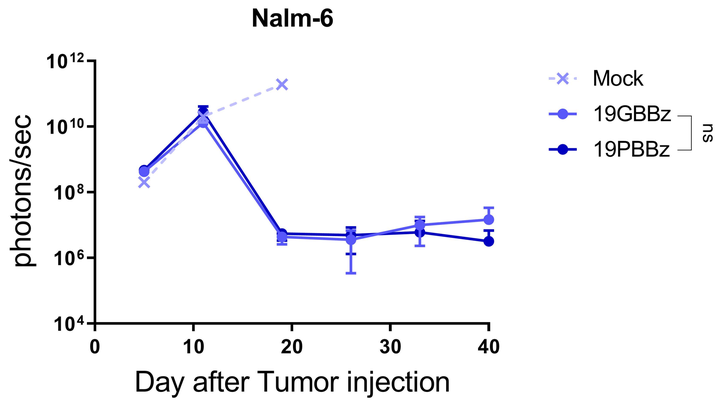

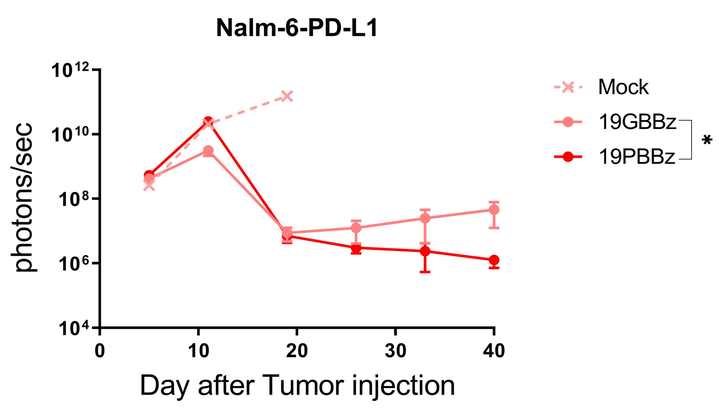

Supplementary figure 3

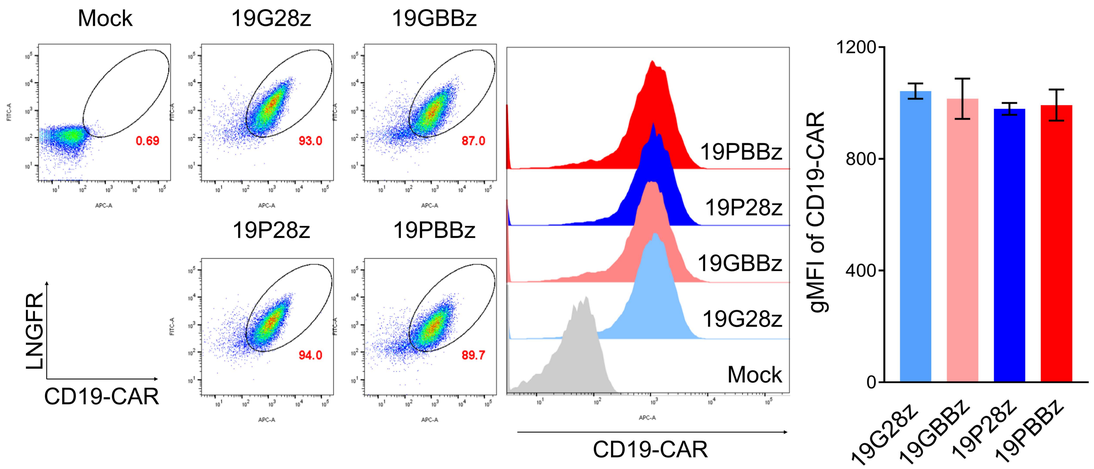

Supplementary figure 4

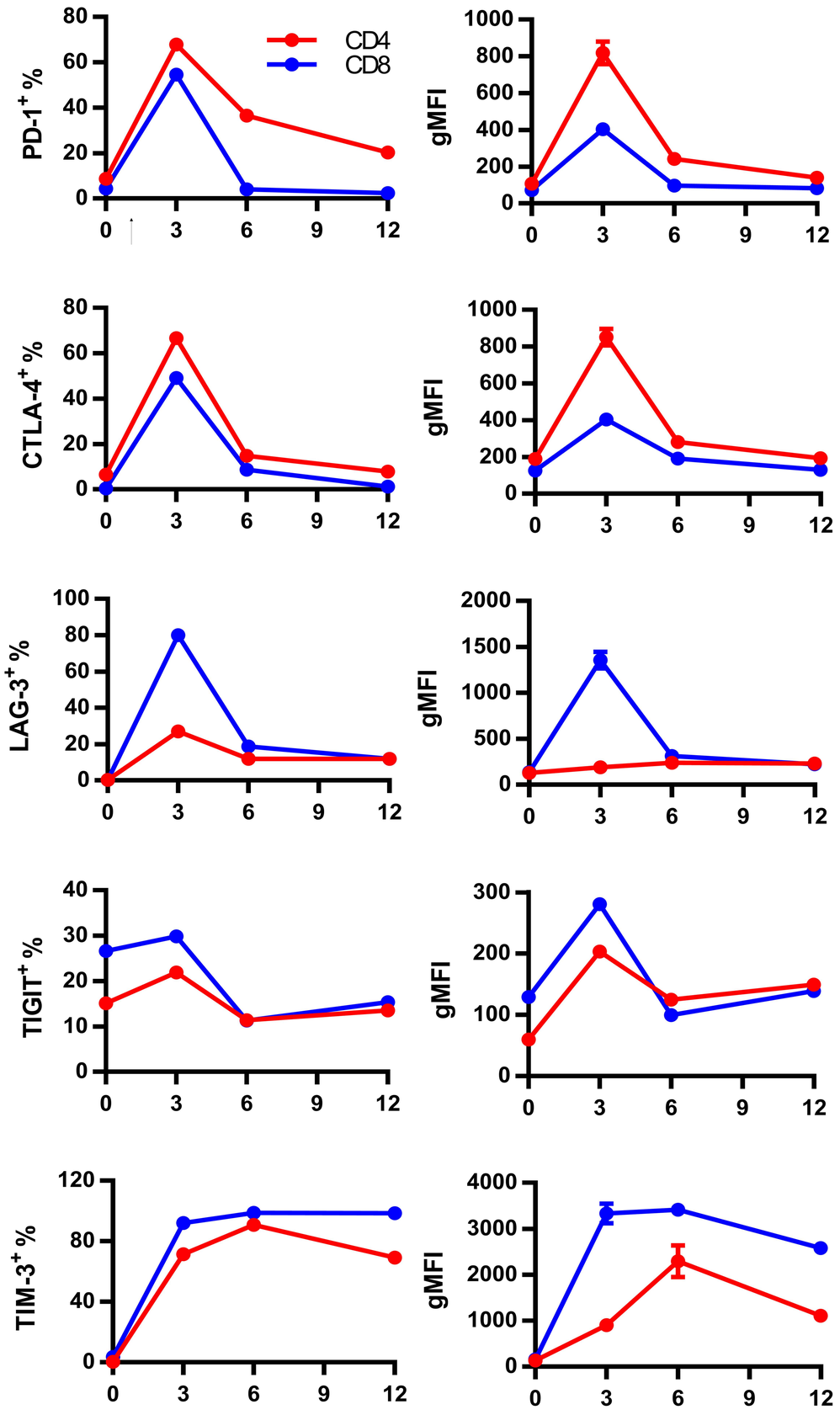

Supplementary figure 5

A

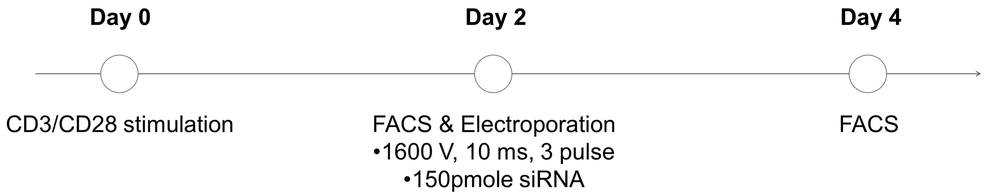

B

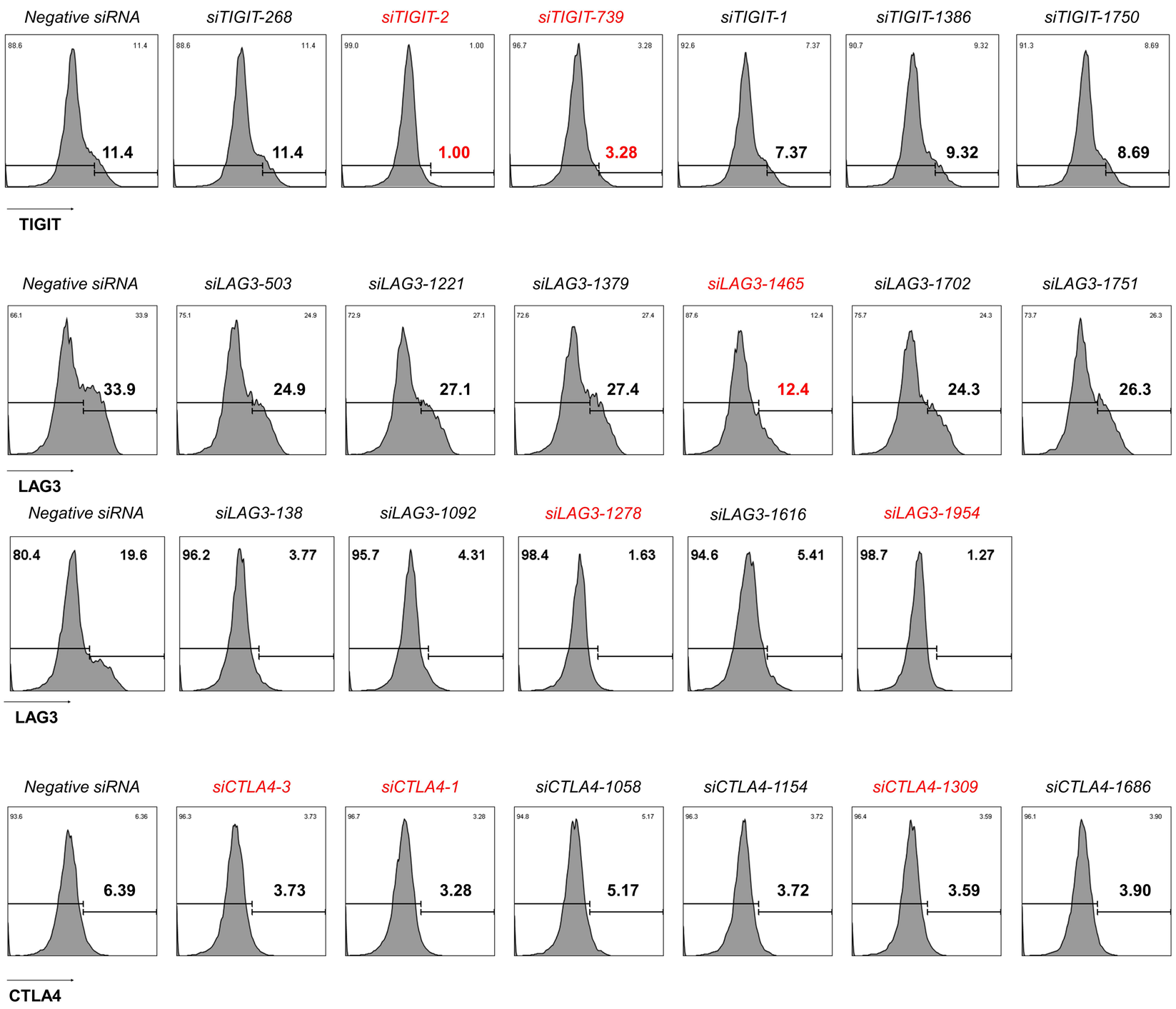

Supplementary figure 6

A

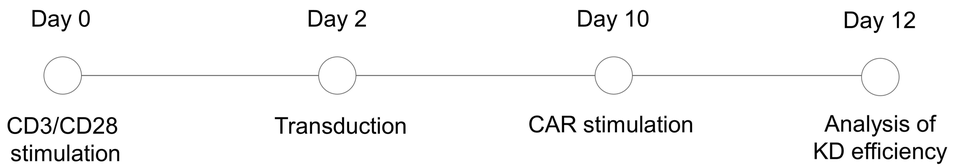

B

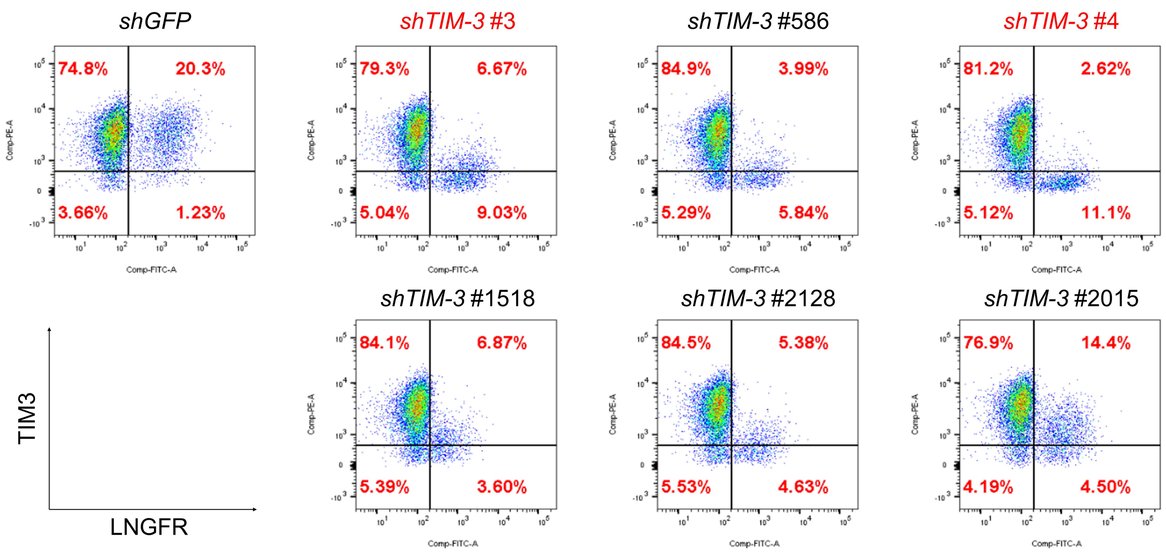

Supplementary figure 7

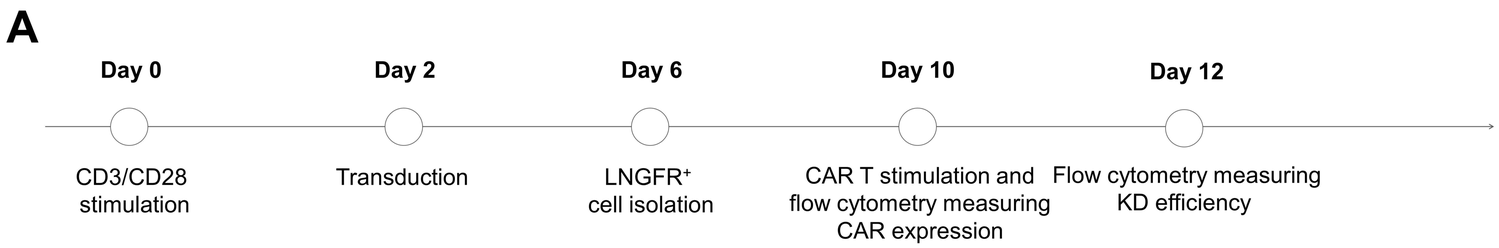

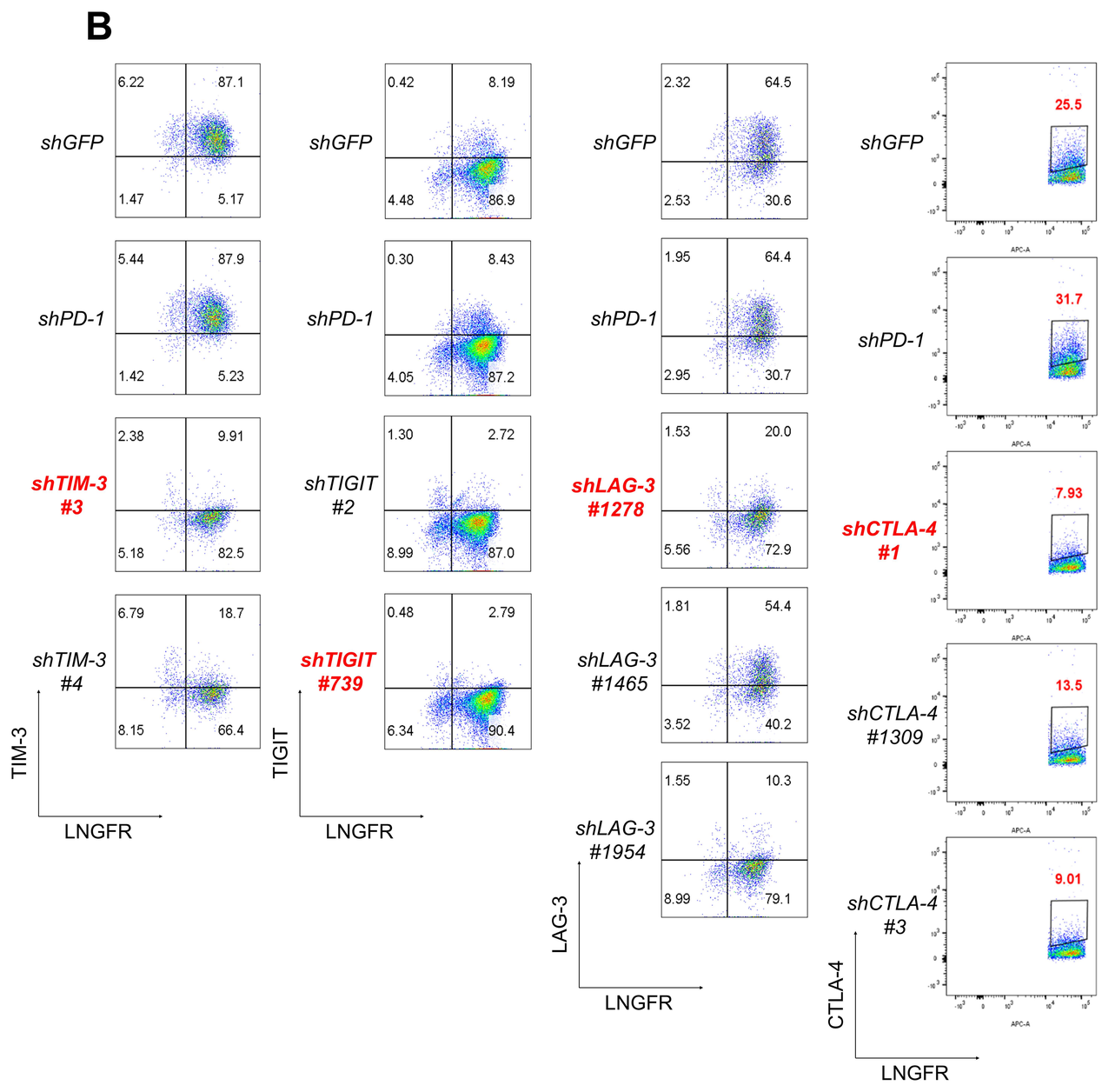

Supplementary figure 8

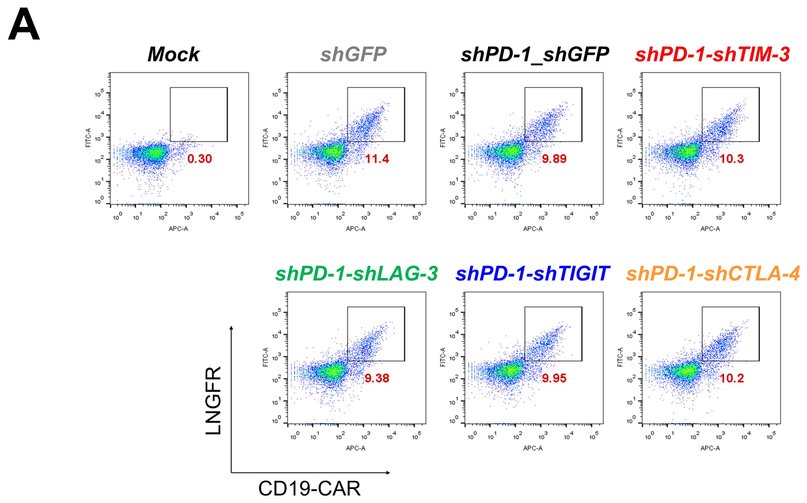

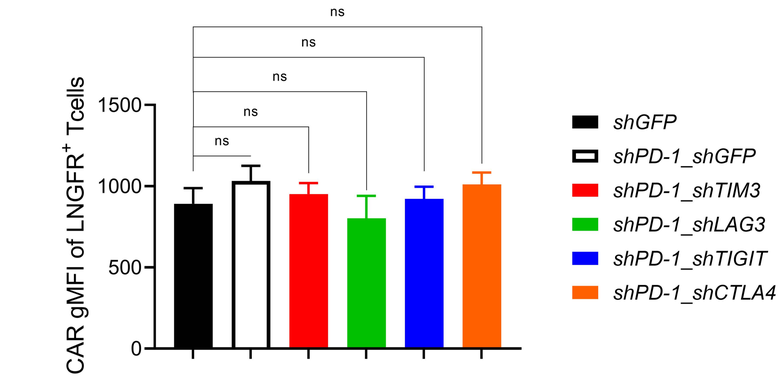

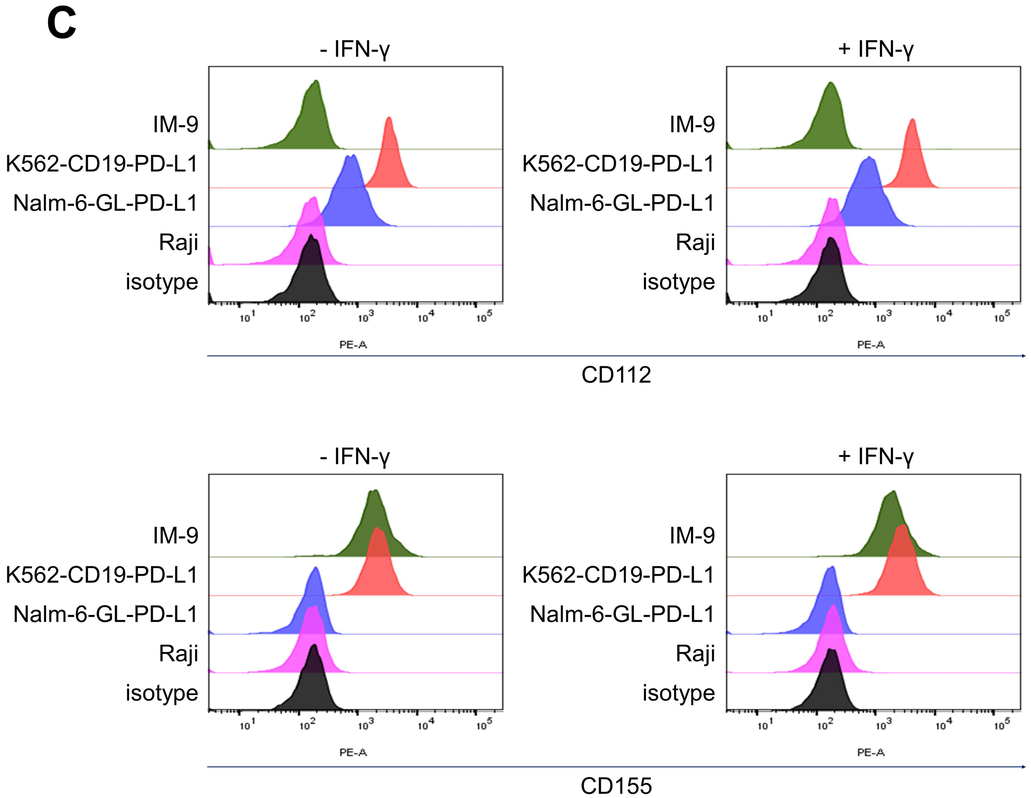

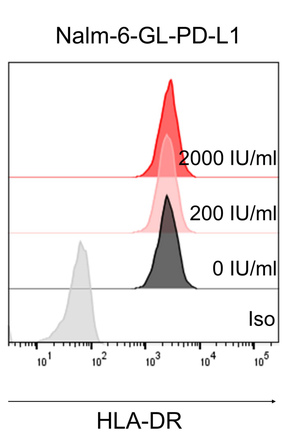

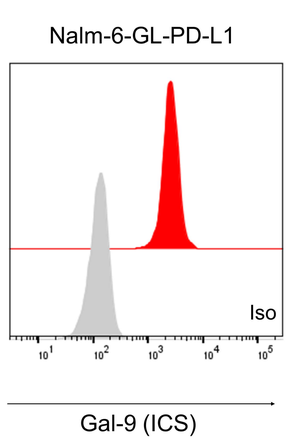

Supplementary figure 9

A

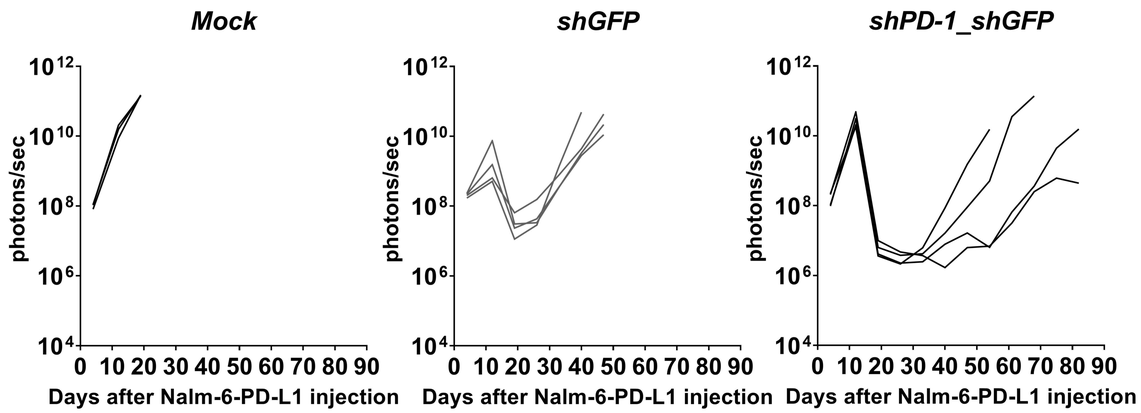

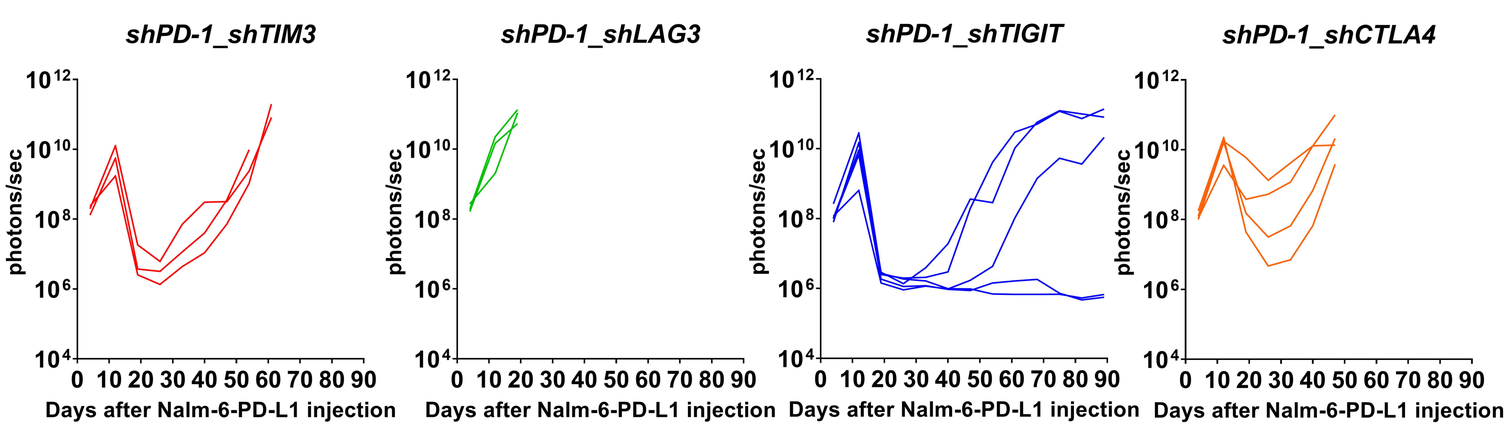

B

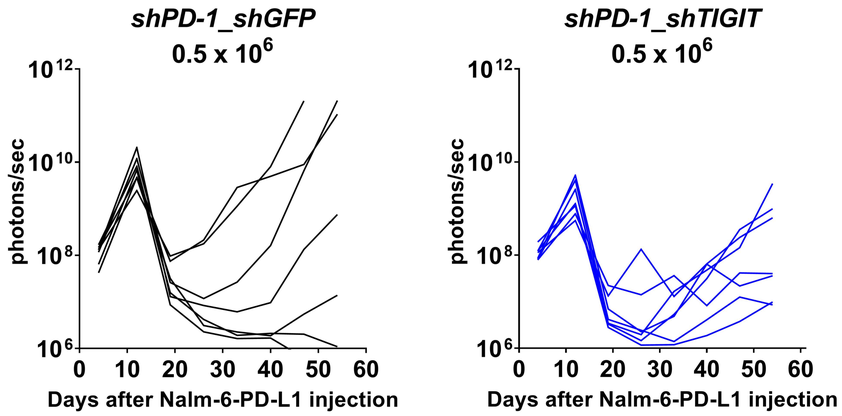

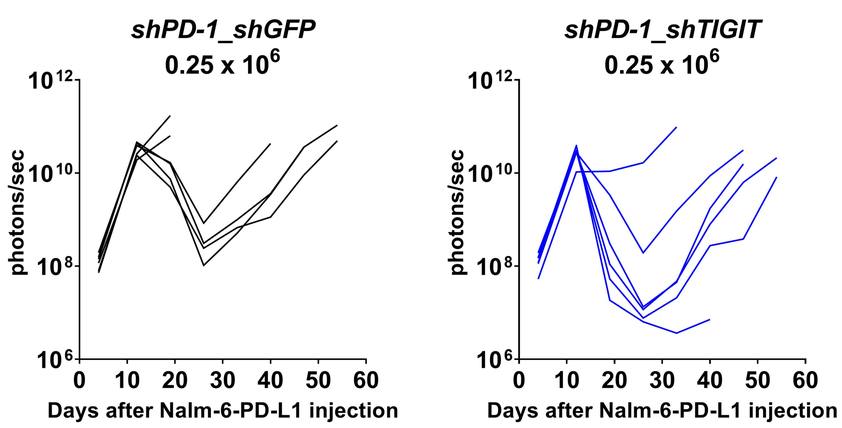

Supplementary figure 10

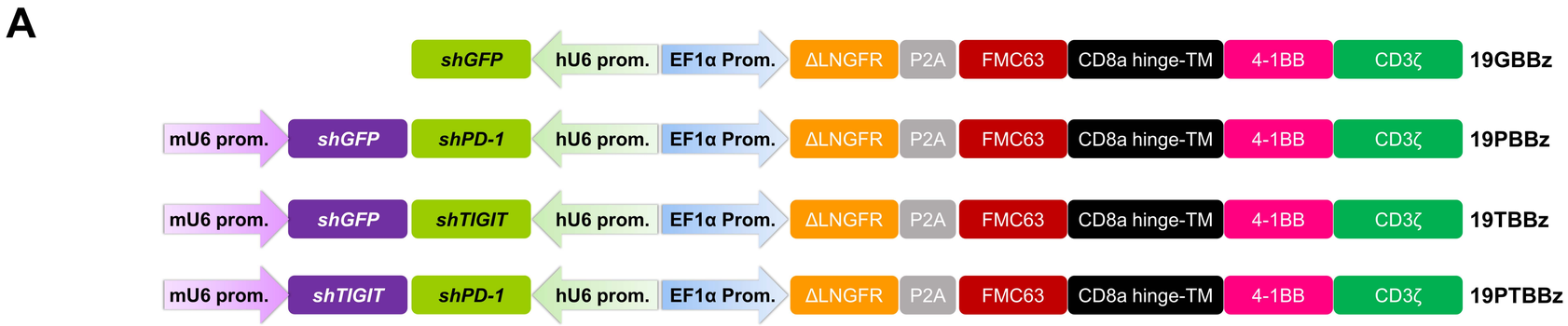

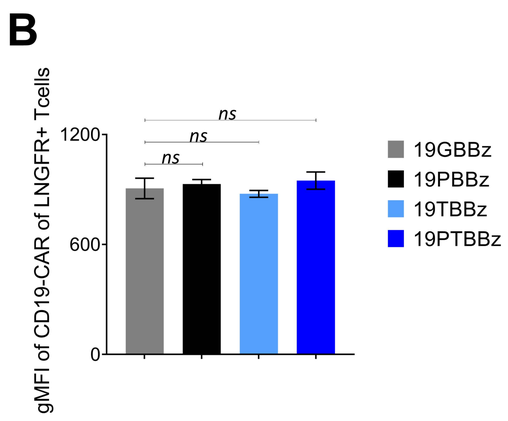

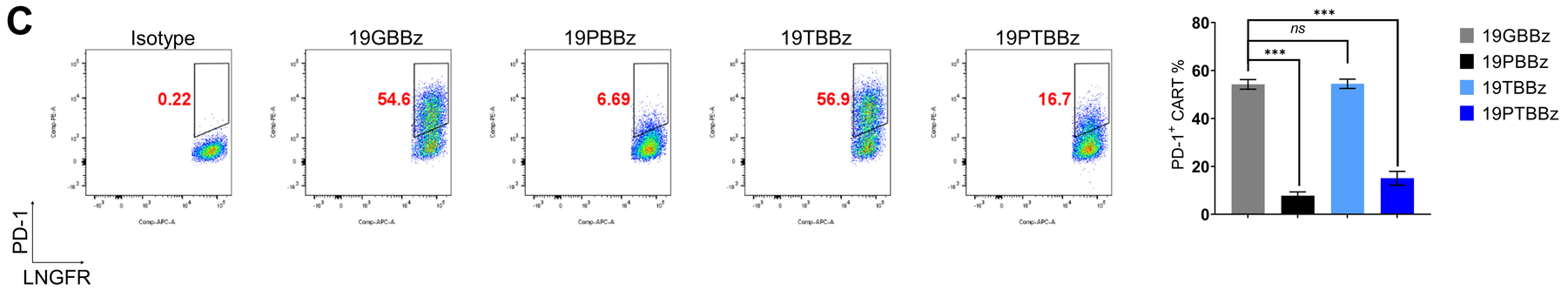

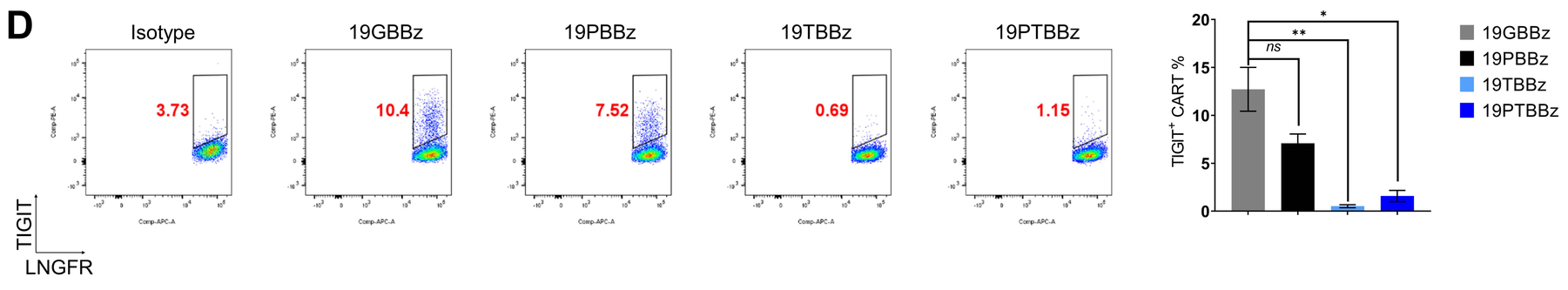

Supplementary figure 11

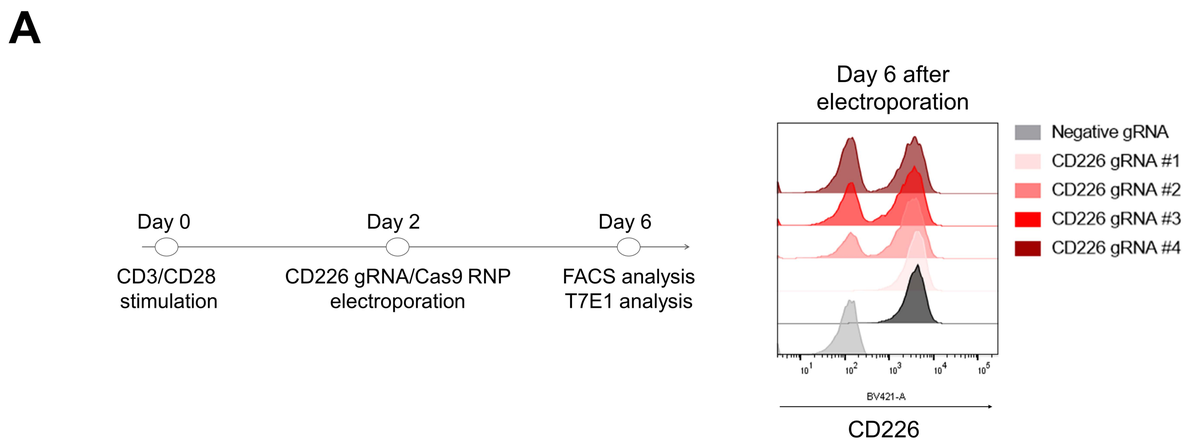

Supplementary figure 12

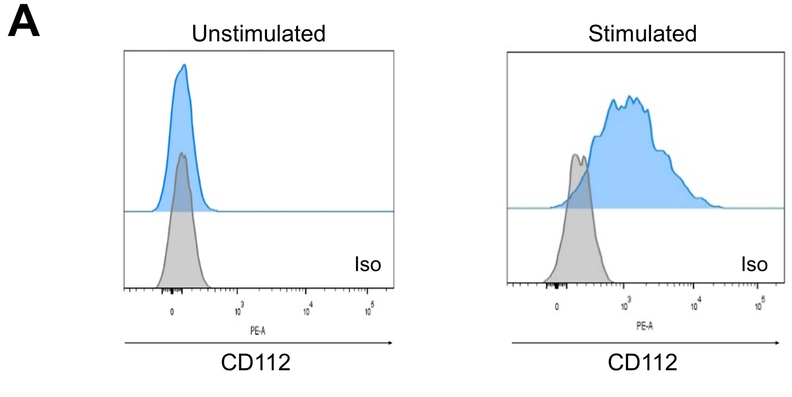

Supplementary figure 13

A

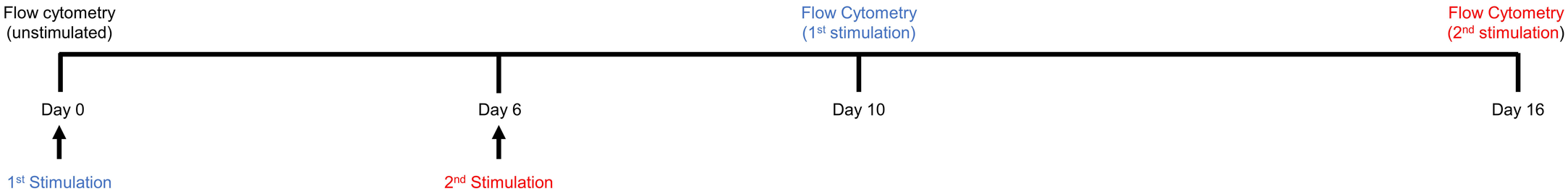

B

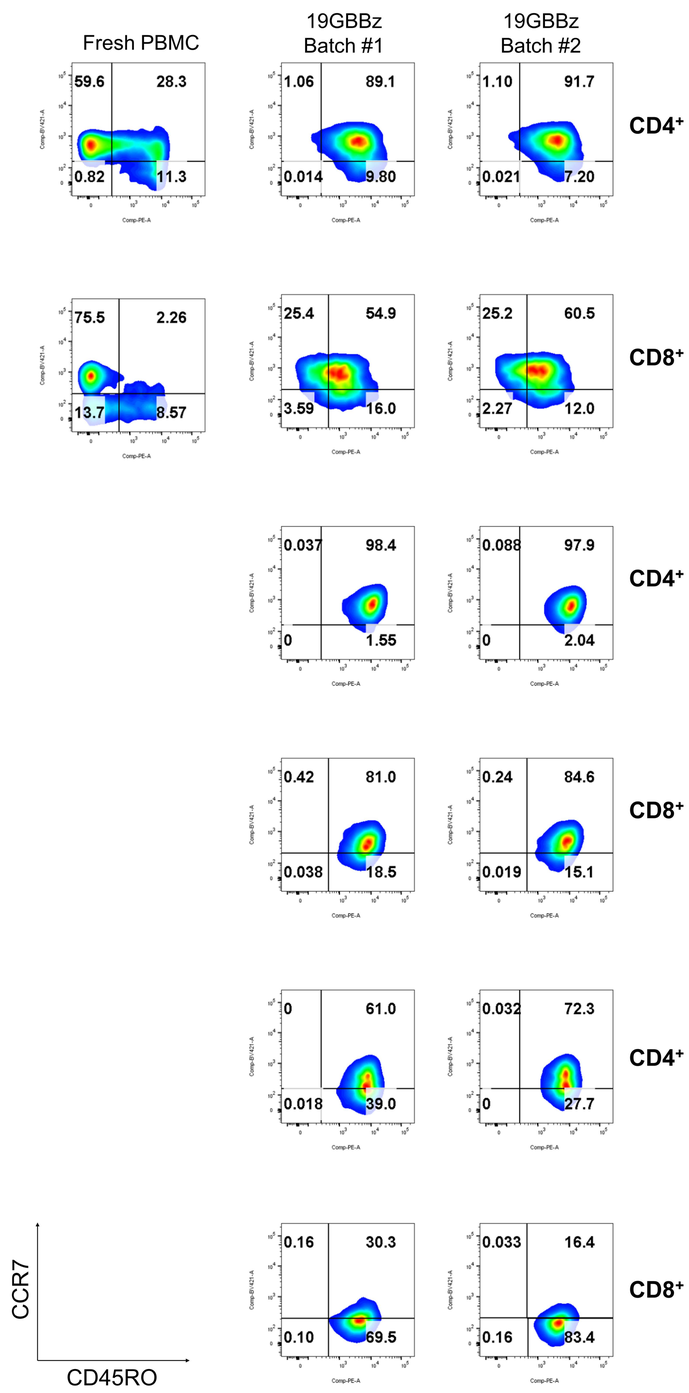

Supplementary figure 14

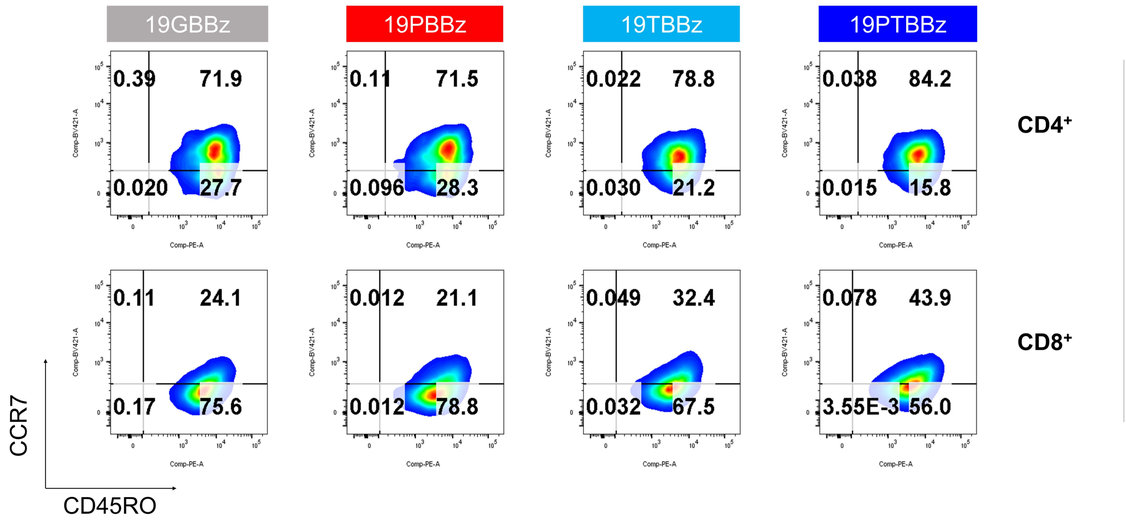

Supplementary figure 15

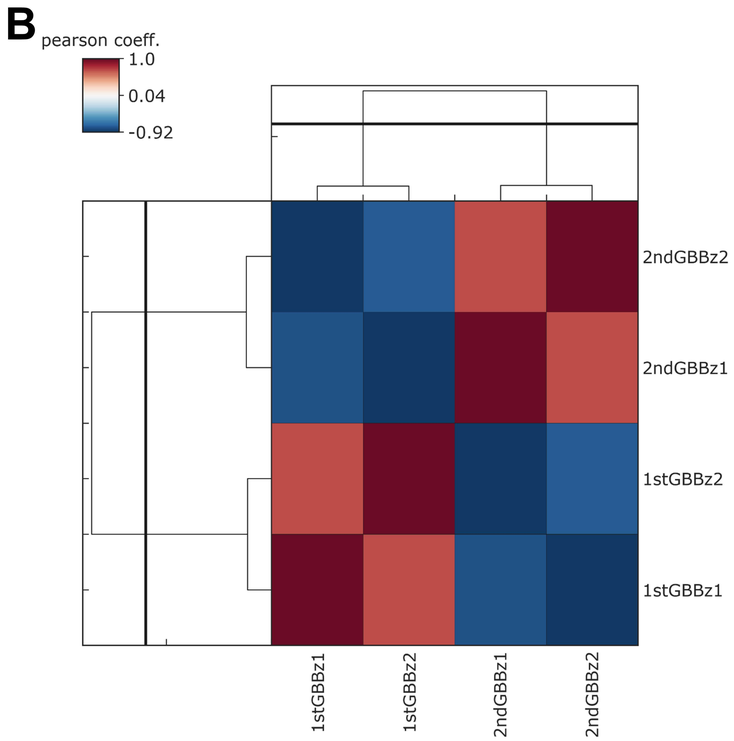

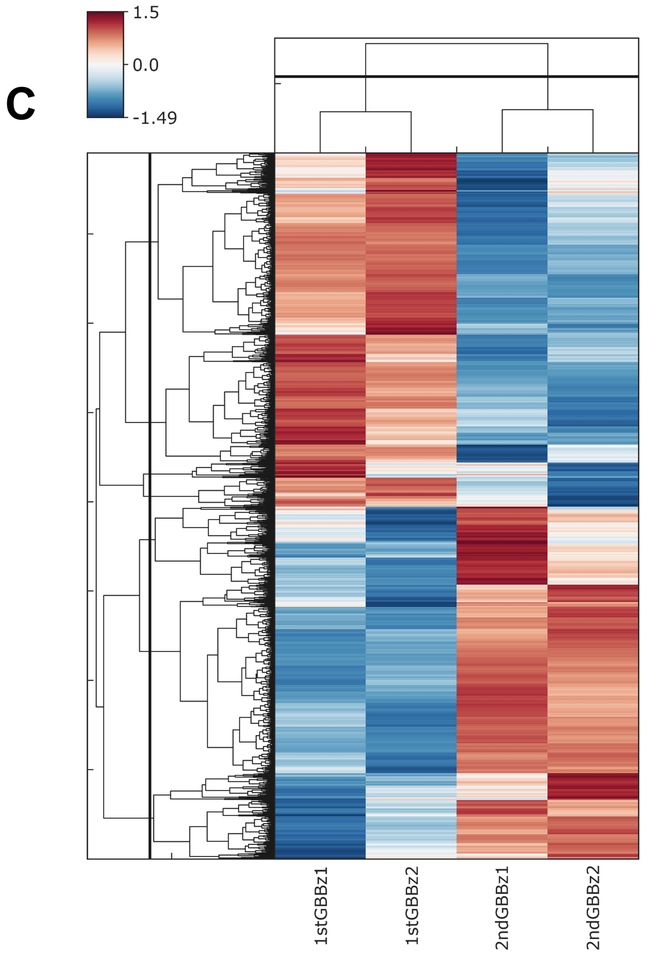

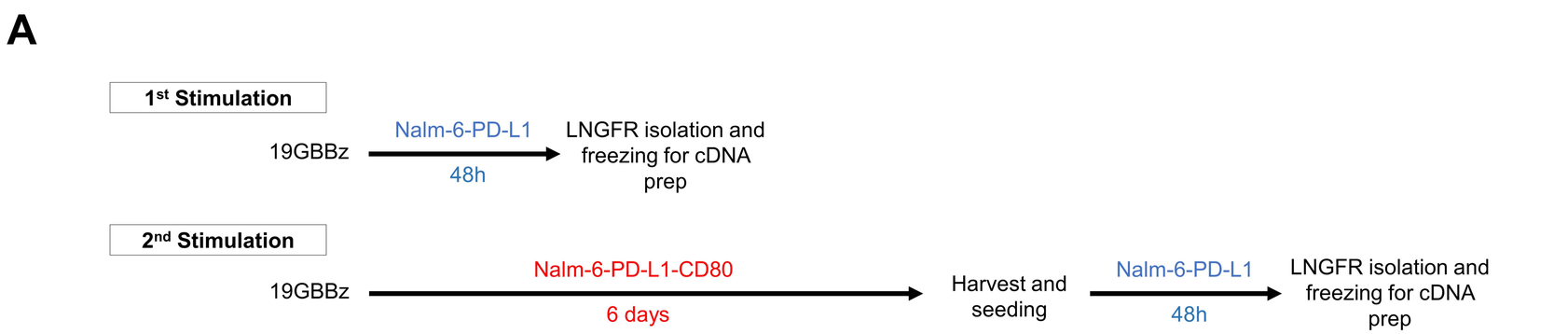

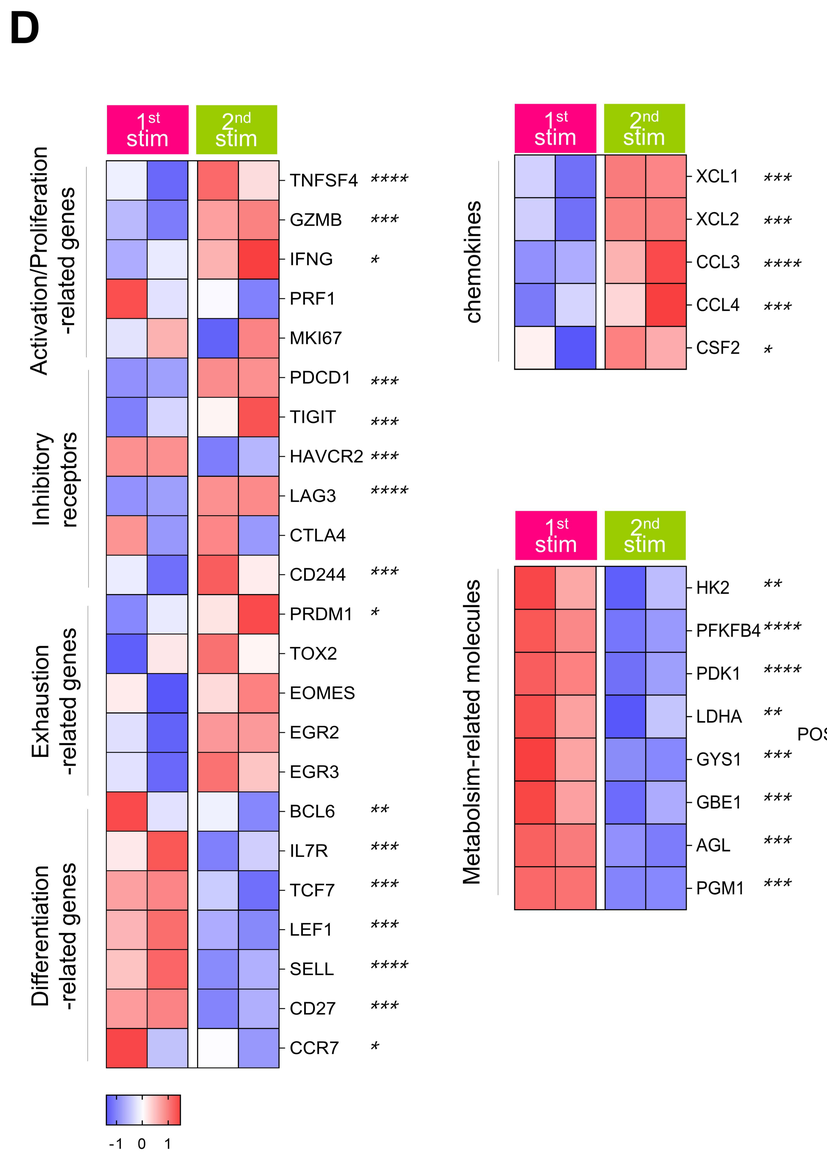

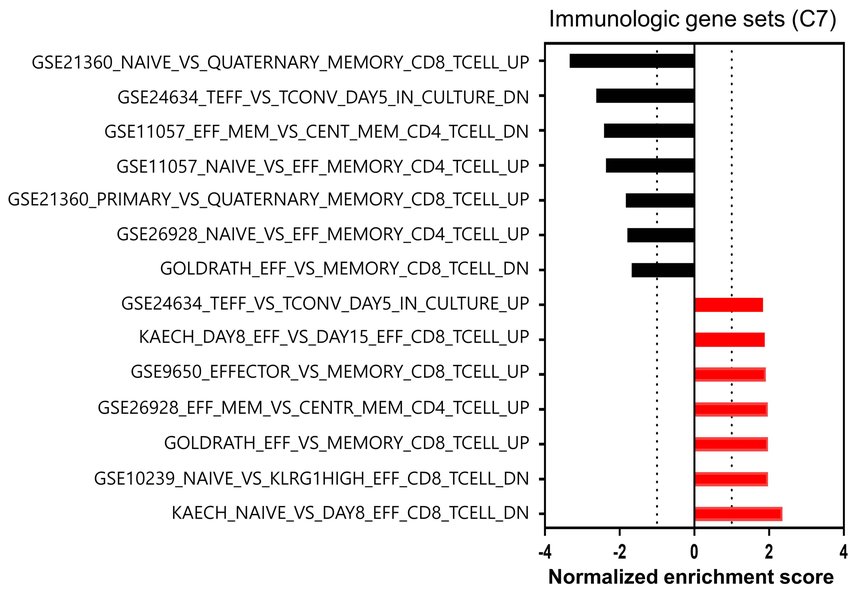

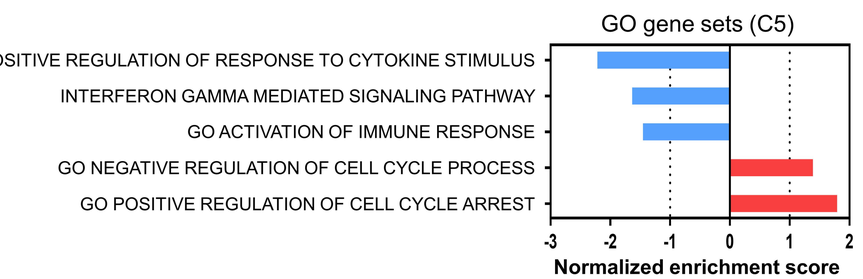

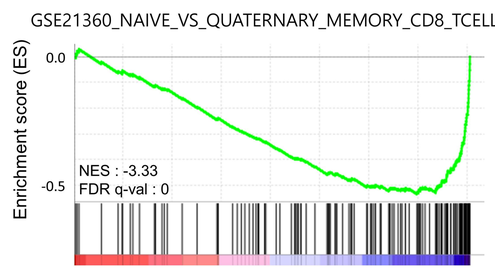

Supplementary figure 16

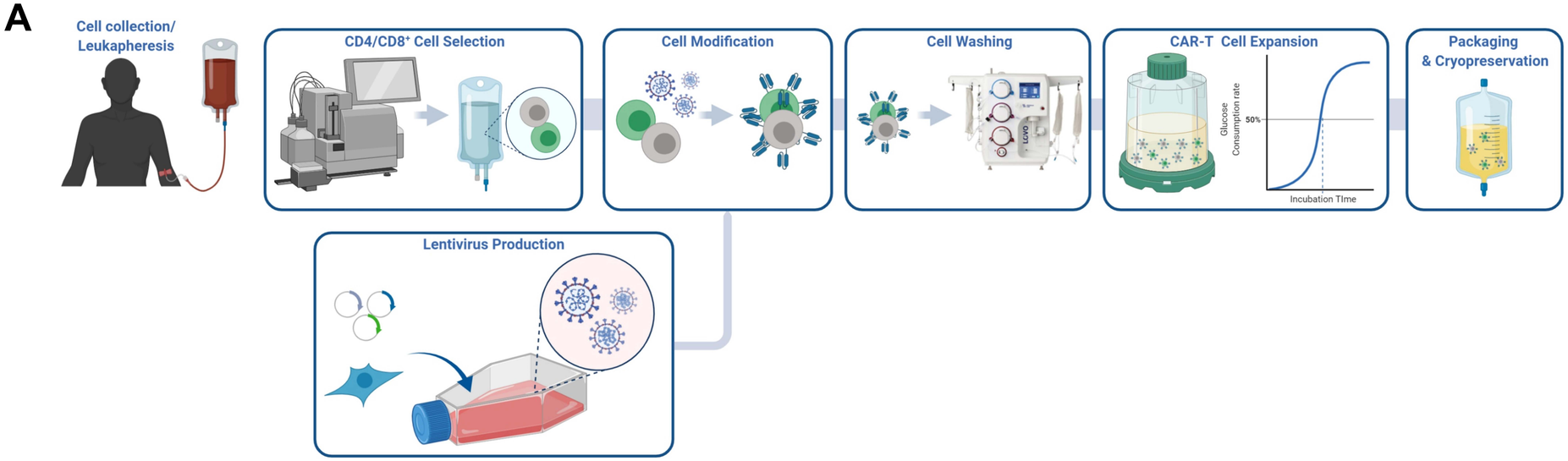

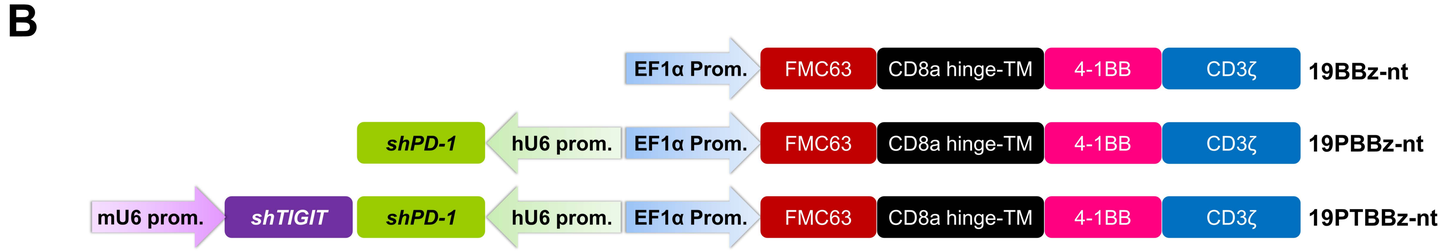

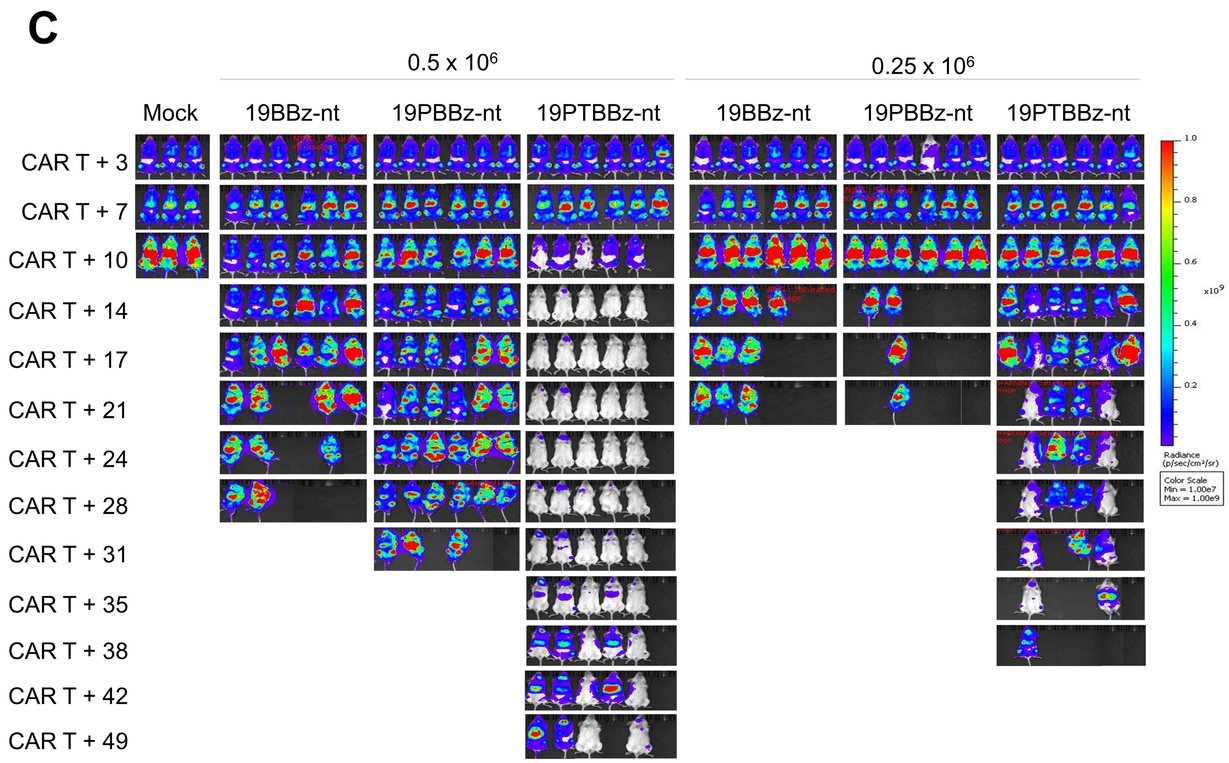

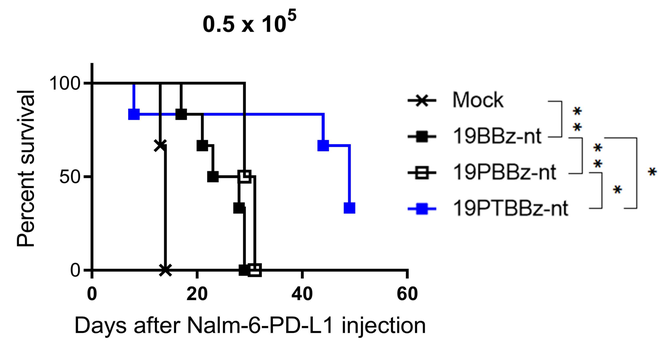

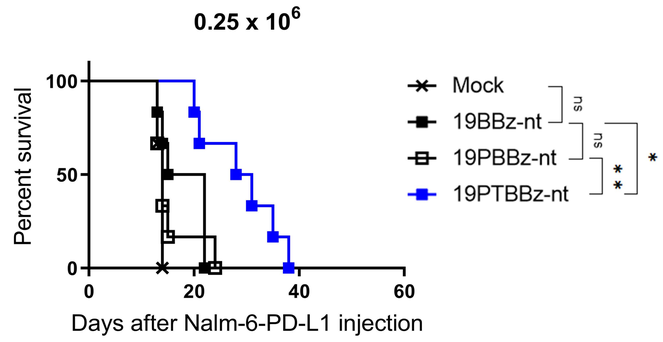

Supplementary figure 17

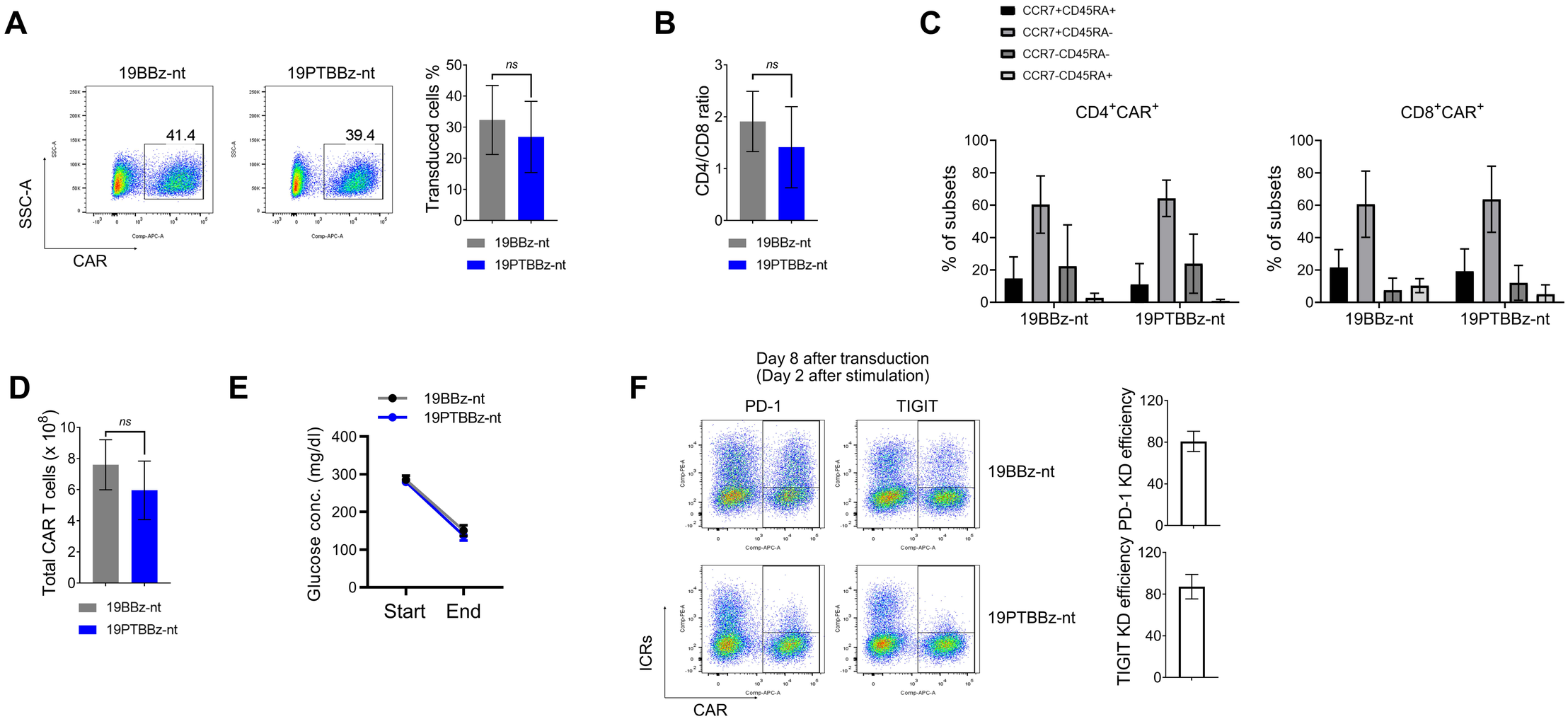

Supplementary figure 18

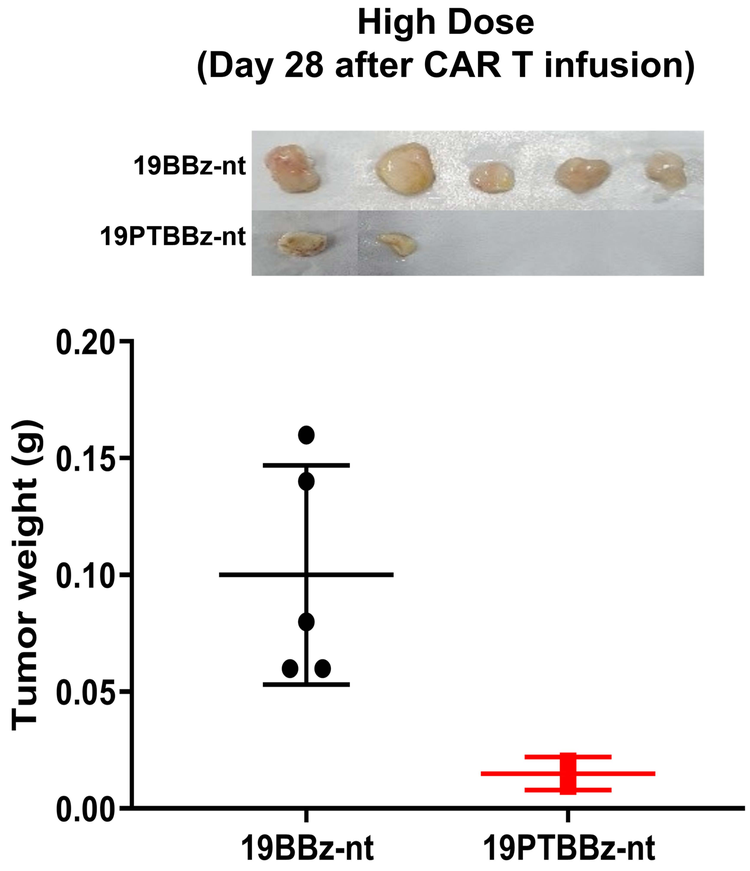

Supplementary figure 19